Journal of Applied Mechanics and Technical Physics, Vol. 46, No. 6, pp. 824–834, 2005

INVESTIGATION OF A GAS FLOW WITH SOLID PARTICLES IN A SUPERSONIC NOZZLE

V. N. Vetlutskii, V. L. Ganimedov, and M. I. Muchnaya

UDC 541.182.8

A two-phase flow with high Reynolds numbers in the subsonic, transonic, and supersonic parts of the nozzle is considered within the framework of the Prandtl model, i.e., the flow is divided into an inviscid core and a thin boundary layer. Mutual influence of the gas and solid particles is taken into account. The Euler equations are solved for the gas in the flow core, and the boundary-layer equations are used in the near-wall region. The particle motion in the inviscid region is described by the Lagrangian approach, and trajectories and temperatures of particle packets are tracked. The behavior of particles in the boundary layer is described by the Euler equations for volume-averaged parameters of particles. The computed particle-velocity distributions are compared with experiments in a plane nozzle. It is noted that particles inserted in the subsonic part of the nozzle are focused at the nozzle centerline, which leads to substantial flow deceleration in the supersonic part of the nozzle. The effect of various boundary conditions for the flow of particles in the inviscid region is considered. For an axisymmetric nozzle, the influence of the contour of the subsonic part of the nozzle, the loading ratio, and the particle diameter on the particle-flow parameters in the inviscid region and in the boundary layer is studied.

Key words: *two-phase flow, viscous flow in the nozzle, numerical methods.*

Introduction. Various gas-particle flows were studied in a number of papers where the gas flow was described by the full Navier–Stokes equations, Euler equations, and boundary-layer equations. The Eulerian approach is commonly used to study the behavior of particles, with all particle parameters being averaged over an elementary volume. A more recent trend is to use the Lagrangian approach where the parameters of each particle or a particle packet are computed.

The flow in the boundary layer on a flat plate with a shock wave passing along the plate was considered in [1–3]. The gas motion was described by the equations of a compressible laminar boundary layer, and the motion of particles was computed by the Euler equations. Velocity and temperature profiles for the gas and particles were presented. Outa et al. [3] compared the numerical results with their own experiments conducted with glass spheres and found that particles 50 μm in diameter are concentrated near the boundary-layer edge.

Saurel et al. [4] used the Euler equations for the gas and particles. It was shown that the equations for particles are degenerate hyperbolic equations, and a special numerical method was proposed to solve them. Results of computations of the flow in a curved channel with injection of particles through the side wall were presented. In [5, 6], the gas flow was computed with the use of the full Navier–Stokes equations. The two-phase flow in a shock tube was studied with allowance for the lifting force for particles.

An unsteady problem for a two-phase flow behind a shock wave passing through a dusty gas in a compression corner was considered in [7]. The motion of both phases was described by the Euler equations. It was shown that

Institute of Theoretical and Applied Mechanics, Siberian Division, Russian Academy of Sciences, Novosibirsk 630090; vetl@itam.nsc.ru; ganim@itam.nsc.ru; mim@itam.nsc.ru. Translated from Prikladnaya Mekhanika i Tekhnicheskaya Fizika, Vol. 46, No. 6, pp. 65–77, November–December, 2005. Original article submitted November 11, 2004; revision submitted January 12, 2005.

the shock wave is decelerated to a greater extent as the dust concentration increases and that the density of particles behind the shock wave decreases with time. Passage of a shock wave through a dusty layer of air above a flat plate was analyzed in [8] with the use of the full Navier–Stokes equations for the gas and the Euler equations for particles. An effect of the lifting force on the particle behavior was identified. Passage of a shock wave above a plane cavity was considered in [9, 10]. In both papers, the flow of the gas and particles was described by the Euler equations. The loading ratio and the particle size were found to exert a significant effect on the flow in the cavity.

In [11–15], the two-phase flow in supersonic nozzles was considered within the framework of the Euler equations for both phases. Various algorithms were suggested for computing both monodisperse and polydisperse flows, with a stiff system of equations for particles. Examples of computations for various configurations of nozzles were given for loading ratios lower than unity.

Sommerfeld [16] computed the exhaustion of a sonic underexpanded gas-particle jet into an ambient space. The gas and particles were computed by the Euler and Lagrange equations, respectively. An algorithm for computing the case with particles of different sizes present in the flow and an algorithm that takes into account particle collisions were proposed. Axial distributions of the gas and particle velocities and temperatures were presented.

Exhaustion of an incompressible turbulent jet was considered experimentally and theoretically in [17]. Parabolized Navier–Stokes equations were used to compute the gas flow, and the behavior of glass spheres was determined by the Lagrange equations. The particle velocity in the jet was measured by the Laser Doppler Velocimetry (LDV). It was demonstrated that particles in a two-phase flow accelerate the gas as compared to a single-phase flow.

Yanenko et al. [18] used LDV to measure the particle velocity at the centerline of the supersonic part of a plane nozzle. The velocity of the gas without particles was measured by LDV and by a Pitot tube. Particles made of different materials were used in experiments, the particle diameters varied almost by an order of magnitude, and the densities of substances and the loading ratio varied by more than an order of magnitude.

In the present work, we considered a gas flow with solid particles in a supersonic nozzle. It was assumed that the Reynolds number was sufficiently high and the boundary-layer thickness was sufficiently small for the entire flow to be divided into an inviscid core and a thin boundary layer. In the first domain, the gas flow was described by the Euler equations, and the motion of particles followed the Lagrange equations. Gas–particle interaction was taken into account under the same assumptions as those used in the above-mentioned papers: there are no chemical reactions between the gas and particles; because of a small volume concentration of particles, their trajectories do not cross each other, and the particles do not interact with each other; all particles are solid spheres of an identical diameter and having a constant temperature over the cross section; each particle has its own trajectory; the Brownian motion of particles and the force of gravity are neglected; gas–particle interaction is determined by the drag force and heat transfer only. In the second domain, we used the boundary-layer equations for the gas and the Euler equations for the particles whose parameters were averaged over an elementary volume (the particles were considered as a continuous medium). The gas and particle parameters computed in the inviscid domain were imposed as conditions at the boundary-layer edge.

Inviscid Flow in the Nozzle. We consider a gas flow with solid particles in the subsonic, transonic, and supersonic parts of a nozzle with a prescribed contour $r = R(x)$; the nozzle-throat radius is denoted by R_*. For the gas, the divergent form of the Euler equations in the variables $\xi = x/R_*$ and $\eta = r/R(x)$ is [16]

$$\frac{\partial W}{\partial \tau} + \frac{\partial}{\partial \xi}\,(J^{-1}F) + \frac{\partial}{\partial \eta}\,(J^{-1}G) = -J^{-1}\Big(\omega\,\frac{G'}{r} + \nu F_p\Big). \tag{1}$$

The value of the parameter $\omega = 1$ corresponds to an axisymmetric flow, and $\omega = 0$ refers to a plane flow; the values $\nu = 1$ and $\nu = 0$ correspond to a two-phase and a single-phase flow, respectively. The following notation is used here:

$$W = J^{-1}\left|\begin{array}{c}\rho\\ m\\ n\\ e\end{array}\right|, \qquad F = \left|\begin{array}{c}\tilde m\\ (m/\rho)\tilde m + \xi_x p\\ (n/\rho)\tilde m + \xi_r p\\ ((e+p)/\rho)\tilde m\end{array}\right|, \qquad G = \left|\begin{array}{c}\tilde n\\ (m/\rho)\tilde n + \eta_x p\\ (n/\rho)\tilde n + \eta_r p\\ ((e+p)/\rho)\tilde n\end{array}\right|,$$

$$G' = \left|\begin{array}{c}n\\ nu\\ nv\\ ((e+p)/\rho)n\end{array}\right|, \qquad F_p = \left|\begin{array}{c}0\\ (F_{\rm part})_x\\ (F_{\rm part})_r\\ u(F_{\rm part})_x + v(F_{\rm part})_r + Q_{\rm part}\end{array}\right|,$$

$$m = \rho u, \qquad n = \rho v, \qquad \tilde{m} = \xi_x m + \xi_r n, \qquad \tilde{n} = \eta_x m + \eta_r n,$$

$$e = \frac{p}{\gamma - 1} + \frac{m^2 + n^2}{2\rho}, \qquad J^{-1} = \begin{vmatrix} x_\xi & x_\eta \\ r_\xi & r_\eta \end{vmatrix}.$$

The parameters ρ, p, e, u, and v are the density, pressure, total energy, and velocity components in the Cartesian (cylindrical) coordinate system x, r. The term J^{-1} is the Jacobian of coordinate transformation, $(F_{\text{part}})_x$ and $(F_{\text{part}})_r$ are the components of the vector of particle-induced forces acting on the gas, and the parameter Q_{part} characterizes the heat transfer between the gas and particles. All gas-dynamic parameters are normalized to critical velocity of sound a_* and density ρ_*.

System (1) was solved under commonly used no-slip conditions on the wall and symmetry conditions at the centerline. In the cylindrical input part of the nozzle, the gas flow was assumed to be isentropic, parallel to the centerline, and having a given pressure p_0 and a given temperature T_0 equal to the corresponding values in the settling chamber. No boundary conditions were imposed at the exit from the supersonic part of the nozzle.

The motion of particles was described by the Lagrangian approach. For convenience of computations, the particles were united into packets with the coordinates ξ_m, η_m $(m = 1, 2, \ldots, M)$; the velocity and temperature of particles in each packet were assumed to be identical. The following equations of motion and heat transfer in dimensionless form were written for the packet [16]:

$$\frac{d\xi_m}{dt} = u_m, \qquad \frac{d\eta_m}{dt} = \frac{1}{R}\,(v_m - \eta_m R' u_m),$$

$$\frac{du_m}{dt} = \frac{3}{4}\,\frac{\rho}{\rho_{\text{part}}}\,\frac{1}{D_{\text{part}}}\,(C_D)_m (u - u_m)|\boldsymbol{U} - \boldsymbol{U}_m|,$$

$$\frac{dv_m}{dt} = \frac{3}{4}\,\frac{\rho}{\rho_{\text{part}}}\,\frac{1}{D_{\text{part}}}\,(C_D)_m (v - v_m)|\boldsymbol{U} - \boldsymbol{U}_m|, \tag{2}$$

$$\frac{dT_m}{dt} = 6\mu\,\frac{c_{\text{part}}}{c_p}\,\frac{1}{\rho_{\text{part}}\,\text{Re}\,D_{\text{part}}^2}\,\frac{\text{Nu}_m}{\text{Pr}}\,(T - T_m).$$

The following notation was used here in addition to that described above: velocity vectors of the gas and the mth packet of particles ($\boldsymbol{U}$ and $\boldsymbol{U}_m$, respectively) gas viscosity μ, specific heat of the gas and the particle substance (c_p and c_{part}, respectively), particle diameter D_{part}, density of the particle substance ρ_{part}, and Reynolds number Re based on the critical parameters of the gas and on the nozzle-throat radius. The drag coefficient of the particles C_D and the Nusselt number for the particles Nu were determined by the relations

$$(C_D)_m = \frac{24}{\text{Re}_m}\Big(1 + \frac{\text{Re}_m^{2/3}}{6}\Big) \quad \text{for} \quad \text{Re}_m < 1000, \qquad (C_D)_m = 0.44 \quad \text{for} \quad \text{Re}_m > 1000,$$

$$\text{Nu}_m = 2 + 0.6\,\text{Re}_m^{1/2}\,\text{Pr}^{\,1/3},$$

where Pr is the Prandtl number for the gas and $\text{Re}_m = \rho D_{\text{part}}|\boldsymbol{U} - \boldsymbol{U}_m|\,\text{Re}\,/\mu$ is the Reynolds number for the particles in the mth packet.

All particles were assumed to be introduced in a certain cross section of the nozzle $\xi = \xi_0$ uniformly over the cross section, with a prescribed velocity and temperature. The packet coordinate within the computational cell was determined by a generator of random numbers, and the number of particles in a packet N_m was determined by the loading ratio ψ equal to the ratio of mass flow rates of the particles and gas.

Interaction between the particles and the nozzle wall can have different forms, depending on properties of the particles and the inner surface of the nozzle. In the present work, we considered three variants of the boundary conditions on the wall: 1) no-slip condition where all particles incident onto the wall were removed from the computation; 2) condition of inelastic interaction where the particles on the wall were deprived of the normal component of velocity; 3) condition of elastic reflection where the sign of the normal component of particle velocity was changed to the opposite one. The condition of symmetry was imposed at the nozzle centerline, which implied that a particle crossing the centerline and leaving the domain considered was replaced by a particle with the same

parameters but with the transverse velocity component of the opposite sign. The boundary at the nozzle exit was not subjected to any boundary conditions.

In the case of inelastic interaction, the particles may accumulate near the wall, and the particle concentration at the centerline can increase owing to particle focusing. The behavior of particles in such a domain was considered in [21] within the framework of the continuum approach; the concepts of a "sheet" and a "string" were introduced for the solid phase. In the present work, the validity of the assumption about the absence of particle collisions with each other was monitored on the basis of the mathematical probability of the absence of collisions P_0 [16]

$$P_0 = \exp\left(-N_c \Delta t\right), \qquad N_c = \frac{(2D_{\text{part}})^2}{V_{jk}} \frac{\pi}{4} \sum_m N_m |\boldsymbol{U} - \boldsymbol{U}_m|, \tag{3}$$

where N_c is the frequency of collisions, V_{jk} is the volume of the difference cell, and Δt is the time of particle residence in this cell. Systems (1) and (2) were solved numerically on a finite-difference grid with cell numbered j along the ξ coordinate and k along the η coordinate. Then, the components of particle-induced forces acting on the gas and the corresponding heat flux can be written as follows [16]:

$$(F_{\text{part}})_x = \frac{\pi}{8V_{jk}} \rho D_{\text{part}}^2 \sum_m N_m (u - u_m)(C_D)_m |\boldsymbol{U} - \boldsymbol{U}_m|,$$

$$(F_{\text{part}})_r = \frac{\pi}{8V_{jk}} \rho D_{\text{part}}^2 \sum_m N_m (v - v_m)(C_D)_m |\boldsymbol{U} - \boldsymbol{U}_m|,$$

$$Q_{\text{part}} = \frac{\pi}{V_{jk}} \frac{\mu}{\text{Re}\,\text{Pr}} \sum_m N_m \,\text{Nu}_m \, D_{\text{part}} (T - T_m).$$

Summation is performed over all packets located in this cell.

Equations (1) were spatially approximated on the basis of a finite-difference TVD scheme developed in [19]. This scheme ensures the second order of approximation on smooth solutions. As this scheme employs a five-point template over each spatial variable, one has to involve two points outside the domain boundary to perform computations in the boundary nodes. The values of the sought functions at these points were found by extrapolation with allowance for the boundary conditions. Soft conditions were imposed at the nozzle exit. The resultant equations containing derivatives with respect to time were solved by a five-step Runge–Kutta method [20], which ensured the second order of accuracy in terms of time. System (2) was integrated by the Euler method. For the right sides to be computed, the gas-dynamic parameters were approximated by the least squares technique from their values at the nodes of the Eulerian grid to the points with the coordinates ξ_m and η_m for each packet.

The entire problem was solved by means of successive approximations. With known values of particle parameters at certain points of the domain, several time steps were made in gas-dynamic equations. Then one step was made in Eqs. (2) with fixed values of gas parameters. After that, Eqs. (1) were solved with new values of particle parameters, and then Eqs. (2) were solved again. This process was continued until the balance of particles in the cross section of their insertion, at the nozzle exit, and deposited on the wall was reached with prescribed accuracy. Stabilization of gas-dynamic parameters was also monitored.

The workability of the generated algorithm was checked by comparing the computed results with experimental data [18]. A plane nozzle had a contoured subsonic part and a straight-line supersonic part with an apex half-angle of 5.5°. The pressure in the settling chamber was 8 bar, and the temperature was 260 K. First, the gas-velocity distribution at the nozzle centerline in the flow without particles was computed and compared with the experimental results. The gas velocity was measured by a Pitot tube. The difference between the computations and experimental data was within 4%.

The next comparison was performed for the flow in the same nozzle but with particles inserted at a temperature of 293 K in the cylindrical part of the nozzle with a velocity equal to the local velocity of the gas. Particles made of different substances and of different diameters were used, as well as different loading ratios. The no-slip condition was chosen in the computations as the boundary condition for particles on the wall. The particle velocity was measured by LDV. The computed and experimental values of particle velocity are plotted in Fig. 1 (in this and subsequent figures, the vertical bar at $\xi = 19$ indicates the nozzle throat). The best agreement with experimental results was obtained in computations for bronze particles (the difference was within 8%), a slightly greater difference was observed for Plexiglas (12%), and the greatest difference was obtained for lycopodium (14%). The latter can

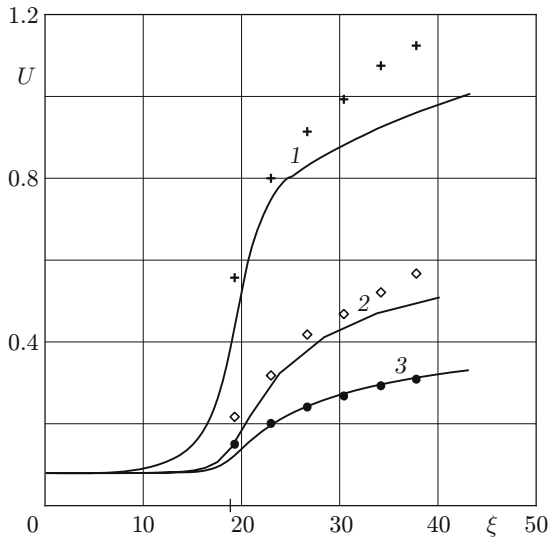

Fig. 1. Computed (curves) and experimental (points) velocity distributions for particles made of different substances at the nozzle centerline: 1) lycopodium ($D_{\text{part}} = 25{\cdot}10^{-6}$ m, $\rho_{\text{part}} = 500$ kg/m^3, and $\psi = 0.316$); 2) Plexiglas ($D_{\text{part}} = 200 \cdot 10^{-6}$ m, $\rho_{\text{part}} = 1200$ kg/m^3, and $\psi = 1.27$); 3) bronze ($D_{\text{part}} = 80 \cdot 10^{-6}$ m, $\rho_{\text{part}} = 8600$ kg/m^3, and $\psi = 4.26$).

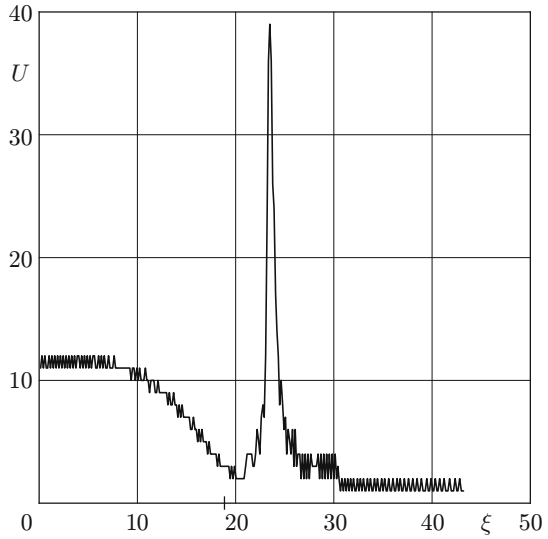

Fig. 2

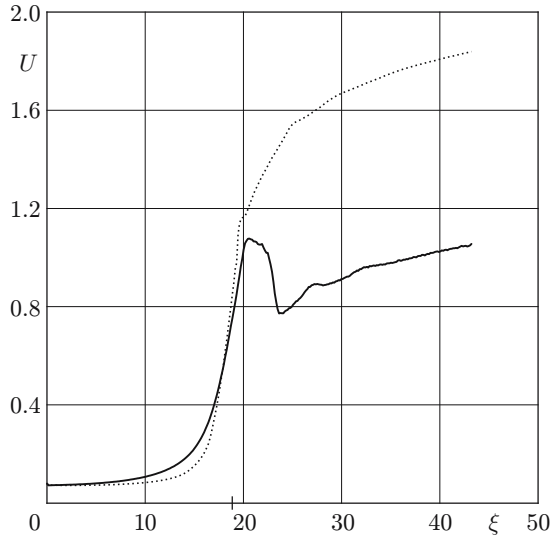

Fig. 3

Fig. 2. Distribution of the number of bronze-particle packets at the nozzle centerline.

Fig. 3. Distribution of gas velocity at the centerline (solid curve) and on the nozzle wall (dotted curve).

be explained by the fact that the surface of lycopodium particles can be significantly different from the spherical shape.

All subsequent computations were performed for gas flows with bronze particles. Figures 2 and 3 show the results computed for the flow in the same nozzle for particles of diameter $D_{\text{part}} = 5 \cdot 10^{-6}$ m with a loading ratio $\psi = 1.0$ for the same governing gas-dynamic parameters. It was found that particles that were not deposited onto the nozzle wall move away from the wall upstream of the nozzle throat and turn toward the nozzle centerline, where the particle concentration significantly increases. This phenomenon is illustrated in Fig. 2, which shows the distribution of density of particle packets along the nozzle centerline. At $\xi = 24$, this quantity increases by an order

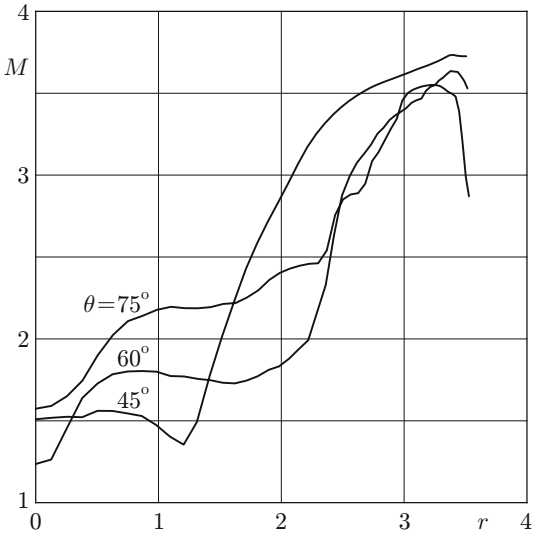

Fig. 4. Distribution of the Mach number at the nozzle exit for different half-angles of its subsonic part.

of magnitude as compared to the neighboring cross sections. The probability of the absence of particle collisions estimated by Eq. (3) yielded $P > 0.999$. Note, the probability of collisions for larger particles is even lower, because the collision frequency N_c is proportional to the particle diameter squared.

A significant increase in particle concentration at the centerline leads to significant deceleration of the gas flow in the supersonic part of the nozzle, which is demonstrated in Fig. 3. The flow velocity becomes supersonic downstream of the nozzle throat, after that the gas is decelerated by particles with the velocity coefficient reaching 0.8 and then is again accelerated to a supersonic velocity. As there are no particles near the wall, the gas velocity monotonically increases in this region.

Interaction of particles with the nozzle surface depends on their mechanical properties, shape, temperature, and other factors. This issue was not considered in the present work, but the influence of different boundary conditions on the wall on the gas–particle flow in the nozzle was examined. For this purpose, three variants of computations for the previously indicated governing parameters (except for the loading ratio equal here to $\psi = 0.5$) were performed: with the no-slip condition (variant I), inelastic interaction condition (variant II), and elastic reflection condition (variant III). The computations showed that the velocity and temperature distributions of the gas and particles in variants II and III are almost coincident. In variant I, the particle velocity in the supersonic part of the nozzle is slightly higher and the temperature is slightly lower than the corresponding values in two other variants. This difference is explained by the fact that, in the first variant, some particles are deposited on the wall, and the number of particles in the supersonic part of the nozzle is smaller than in the other variants.

It turned out that the effect of the boundary conditions on the velocity and temperature distributions of particles at the nozzle exit is more pronounced. The boundary of the particle flux in the first two variants is less than one half of the nozzle height, whereas it reaches two thirds in the last variant. Moreover, the particle velocity and temperature in the second variant are almost constant over a distance of approximately one third of the radius from the nozzle centerline.

The effect of the subsonic part of the nozzle, particle diameter, and loading ratio was considered by an example of an axisymmetric nozzle with a conical supersonic part, half-angle of 15°, and throat radius $R_* = 0.01$ m. The pressure in the settling chamber was 20 bar, the temperature was 500 K, the particle temperature at the nozzle entrance was 293 K, and the particle velocity was assumed to be equal to the gas velocity at the centerline in the entrance cross section of the nozzle. The half-angle of the conical subsonic part of the nozzle varied within $\theta = 30$–$75°$, the particle diameter was $D_{\text{part}} = 25$–100 μm, and the loading ratio was $\psi = 0.2$–1.0. The condition of inelastic interaction was imposed at the boundary. Figure 4 shows the distribution of the Mach number at the nozzle exit for $D_{\text{part}} = 100$ μm, $\psi = 1.0$, and different values of the angle θ. This parameter characterizes the intensity of gas deceleration by particles, in other words, the particle distribution over the nozzle cross section. For

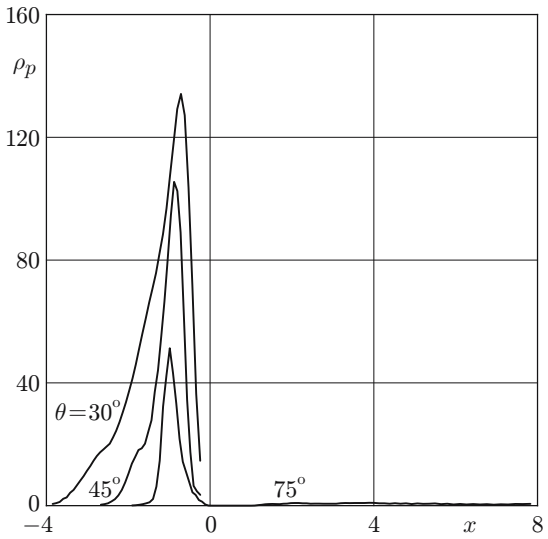

Fig. 5. Distribution of mean density of bronze particles at the boundary-layer edge for different half-angles of the subsonic part of the nozzle.

$\theta = 45°$, the particles are almost uniformly focused within one third of the radius near the nozzle centerline. For large angles of the subsonic part, the particle-laden jet expands at the exit to two thirds of the radius; the particle concentration near the centerline is somewhat higher. Moreover, for $\theta = 75°$, in contrast to other variants, the particles are also present in the vicinity of the wall.

The dependence of the Mach number at the nozzle exit on the particle diameter for $\theta = 60°$, $\psi = 0.2$, and $D_{\text{part}} = 50$, 75, and 100 μm was also considered. In all three variants, the particle-laden jet occupies approximately one half of the radius, with the particle concentration increasing toward the centerline. As it could be expected, with decreasing particle diameter and unchanged mass flow rate, the gas–particle interaction becomes more intense, which leads to more significant deceleration of the gas.

For subsequent computations of the gas–particle flow, the density, velocity, and temperature of particles were averaged over an elementary volume at the boundary-layer edge. Figure 5 shows the distribution of the mean density of particles at the boundary-layer edge for $\theta = 30$, 45, and 75°, $\psi = 0.2$, and $D_{\text{part}} = 100$ μm. The x coordinate is counted here from the nozzle throat. It is seen that the density in the subsonic part of the nozzle drastically increases first and then rapidly decreases, and the particles leave the region of the boundary-layer edge. In the supersonic part of the nozzle, the particles do not fall onto the boundary-layer edge (except for the variant with the maximum value of the angle θ), and their density here is $\rho \approx 10$. The result of gas deceleration near the wall by these particles is demonstrated in Fig. 4.

Boundary-Layer Flow. The effects of gas viscosity and heat conduction are taken into account in the present work in a thin boundary layer on the nozzle surface. As the flow in the supersonic part of the nozzle can be accompanied by shock waves [22] and possible separation of the boundary layer, this problem was solved by the pseudotransient method [23]. The equations of an unsteady compressible boundary layer for the gas–particle flow are written in a surface-fixed coordinate system:

$$\frac{\partial \rho}{\partial t} + \frac{\partial}{\partial \xi}(\rho u) + \frac{\partial}{\partial \eta}(\rho v) + \omega \frac{R'}{R}\rho u = 0,$$

$$\rho \frac{\partial u}{\partial t} + \rho u \frac{\partial u}{\partial \xi} + \rho v \frac{\partial u}{\partial \eta} = -\frac{\partial p}{\partial \xi} + \frac{\partial}{\partial \eta}\Big(\mu \frac{\partial u}{\partial \eta}\Big) + D_x,$$

$$\rho c_p \frac{\partial T}{\partial t} + \rho u c_p \frac{\partial T}{\partial \xi} + \rho v c_p \frac{\partial T}{\partial \eta} = u \frac{\partial p}{\partial \xi} + (\gamma - 1)\Big[\mu\Big(\frac{\partial u}{\partial \eta}\Big)^2 + \Phi\Big] + \frac{1}{\text{Pr}} \frac{\partial}{\partial \eta}\Big(k \frac{\partial T}{\partial \eta}\Big) + Q, \tag{4}$$

$$\rho = \gamma p / T.$$

The coordinates ξ and η are directed along the surface and perpendicular to it, with the corresponding velocity components u and v; μ, k, and c_p are the coefficients of viscosity, thermal conductivity, and specific heat. Michel's algebraic model of turbulence is used for the turbulent flow. All parameters are normalized to their critical values, as in inviscid equations. In addition, the parameters η and v are multiplied by the square root from the Reynolds number Re.

The Eulerian approach was used for the particle flux in the boundary layer [1–3], where the density, velocity, and temperature of particles were averaged over the volume. The two-dimensional steady Euler equations for particles are written in the form

$$\frac{\partial}{\partial\xi}(\rho_p u_p) + \frac{\partial}{\partial\eta}(\rho_p v_p) + \omega\frac{R'}{R}\rho_p u_p = 0,$$

$$\rho_p u_p\frac{\partial u_p}{\partial\xi} + \rho_p v_p\frac{\partial u_p}{\partial\eta} = -D_x, \qquad \rho_p u_p\frac{\partial v_p}{\partial\xi} + \rho_p v_p\frac{\partial v_p}{\partial\eta} = -D_y, \tag{5}$$

$$\rho_p u_p c_{\text{part}}\frac{\partial T_p}{\partial\xi} + \rho_p v_p c_{\text{part}}\frac{\partial T_p}{\partial\eta} = -Q,$$

where ρ_p, u_p, v_p, and T_p are the mean density, velocity components, and temperature of particles. In Eqs. (4) and (5), we introduced the components of the force of particles acting on the gas D_x and D_y, the work of these forces Φ, and the heat flux from the particles to the gas Q, for which we used the following expressions [2]:

$$D_x = \frac{3}{4}\frac{\rho_p\rho}{\rho_{\text{part}}D_{\text{part}}}C_D(u_p-u)|\boldsymbol{U}-\boldsymbol{U}_p|, \qquad D_y = \frac{3}{4}\frac{\rho_p\rho}{\rho_{\text{part}}D_{\text{part}}}C_D(v_p-v)|\boldsymbol{U}-\boldsymbol{U}_p|,$$

$$\Phi = (u_p-u)D_x + \frac{1}{\text{Re}}(v_p-v)D_y, \qquad Q = 6c_p\frac{\rho_p\mu}{\rho_{\text{part}}D_{\text{part}}^2}\frac{\text{Nu}}{\text{Pr Re}}(T_p-T). \tag{6}$$

Here $\boldsymbol{U}$ and $\boldsymbol{U}_p$ are the velocity vectors of the gas and particles. Standard formulas are used for the drag coefficient C_D and Nusselt number Nu.

Nevertheless, it is impossible to construct the solution in the boundary layer in this formulation, because, in the absence of particles, the convective terms for the gas and the pressure gradient gradually acquire the equilibrium with each other when approaching the boundary-layer edge. Therefore, the velocity profile tends asymptotically to its value at the boundary-layer edge. A similar situation is observed for the temperature distribution. In the gas flow with solid particles, however, the parameters of the latter display a principally different behavior: they do not tend asymptotically to certain values at the boundary-layer edge. Therefore, the gas–particle interaction parameters (6), generally speaking, do not tend to zero at the boundary-layer edge, and their allowance in system (4) violates the asymptotic character of gas velocity and temperature. For this reason, we decided to ignore the action of particles on the gas in the boundary layer and to take into account only the influence of the gas on the particles. This assumption is valid only if the particle concentration is rather low.

The gas in the vicinity of the wall is subjected to conventional no-slip and constant-temperature conditions, and the distributions of pressure, streamwise velocity component, and temperature, which are taken from inviscid computations of the gas–particle flow in this nozzle, are imposed on the boundary-layer edge:

$$\eta = 0: \quad u = v = 0,\ T = T_{\text{w}}, \qquad \eta = \eta_e(\xi): \quad p = p_e(\xi), \quad u = u_e(\xi), \quad T = T_e(\xi).$$

A self-similar solution of the boundary layer under given conditions was constructed at the nozzle entrance.

In formulating the boundary conditions for Eqs. (5), we had to study their characteristic properties. We can easily see that this system has the only characteristic of multiplicity equal to four with an inclination $\lambda_{1,2,3,4} = u_p/v_p$, which corresponds to the particle streamline. Yet, the matrix corresponding to this characteristic number has a rank equal to unity; hence, only three linearly independent eigen vectors correspond to this number. Thus, system (5) is not hyperbolic in the common sense [24]. A similar result was obtained in [13, p. 151], where relations on characteristics were written. This system was called in [4] the degenerate hyperbolic system. Unfortunately, the properties of such systems have not been adequately studied; therefore, the boundary-value problem was posed in a manner corresponding to hyperbolic equations. As the flux of particles enters the nozzle through the boundary-layer edge, all four parameters should be set there (density, two components of velocity, and temperature). In this case,

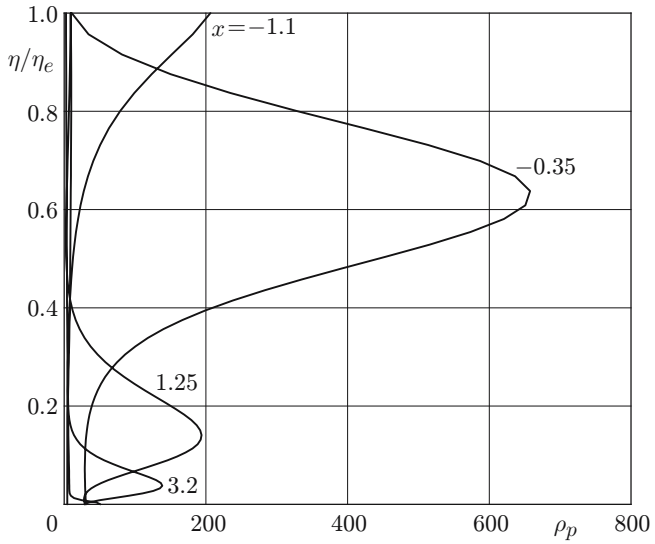

Fig. 6. Profiles of the mean density of bronze particles in the boundary layer at different distances from the nozzle throat.

no conditions are imposed on the nozzle wall. A similar formulation of the boundary conditions was proposed in [25] for an incompressible boundary layer with particles:

$$\eta = \eta_e(\xi): \quad \rho_p = \rho_{pe}(\xi), \quad u_p = u_{pe}(\xi), \quad v_p = v_{pe}(\xi), \quad T_e = T_{pe}(\xi).$$

The distributions of parameters are also taken from the computations of a particle-laden inviscid gas flow in this nozzle. In the cross section where the particles were inserted, all their parameters were assumed to be constant over the cross section, as in the inviscid flow.

In Eqs. (4) and (5), for convenience of computations, we introduced the Blasius variable $\lambda = \eta/\sqrt{\xi}$ instead of the coordinate η and performed extension for both independence variables ξ and λ, which was constant for the first variable and solution-dependent for the second one [26]. The boundary-layer equations (4) were solved by an implicit difference scheme [26] until they became time-independent, and the equations for the particles (5) were solved by a through-count difference scheme. Under prescribed conditions at the boundary-layer edge, each of these systems was solved consecutively until the entire process was stabilized.

The particle-laden boundary layer was computed for an axisymmetric nozzle described above and for the same values of the governing parameters. In addition, the wall temperature ($T_{\rm w} = 293$ K) and the Reynolds number ($\mathrm{Re} = 1.52 \cdot 10^6$) based on the critical parameters were set. It was assumed that the flow is laminar at first and becomes turbulent at a distance between three and four throat radii.

Figure 6 shows the profiles of the mean density of particles in the boundary layer for $\theta = 75°$, $\psi = 1$, and $D_{\rm part} = 100$ μm. The numbers at the curves indicate the distance from the nozzle throat. In this variant, the density at the boundary-layer edge reaches a maximum at $x \approx -1.0$, after which these particles penetrate into the boundary layer and move together with the viscous gas flow. As the cross-sectional area through which the gas and particles flow in the boundary layer on the subsonic part of the nozzle decreases severalfold owing to a decrease in the layer thickness and nozzle radius and the particle velocity changes only weakly, the mean density becomes significantly higher in this region. The maximum of density approaches the nozzle surface and decreases in magnitude. (Thus, all particles from the boundary layer are gradually deposited on the wall in the supersonic part of the nozzle.)

The influence of the half-angle of the subsonic part of the nozzle on the distribution of the particle density on the wall for $\theta = 45$, 60, and 75°, $\psi = 0.2$, and $D_{\rm part} = 100$ μm is plotted in Fig. 7. The density drastically increases at first, following its increase on the boundary-layer edge with a certain delay. After that its values decrease at the laminar portion of the supersonic part of the nozzle and then increase and reach an almost constant value. The values of density over the entire length decrease with increasing half-angle, which is explained by a corresponding decrease in density at the boundary-layer edge.

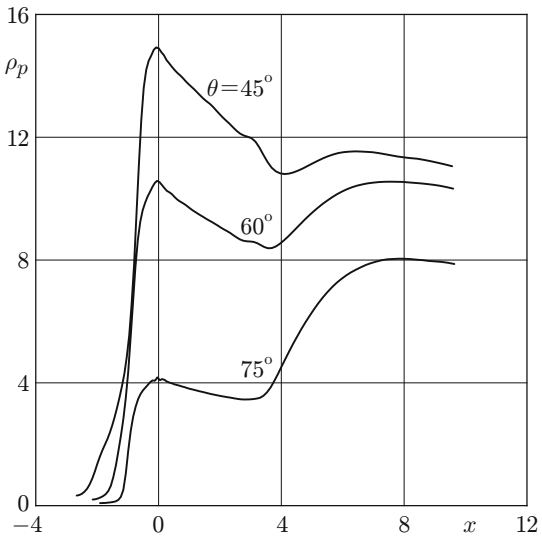

Fig. 7. Distribution of the mean density of bronze particles on the nozzle wall for different half-angles of the subsonic part of the nozzle.

A similar comparison of the particle-density curves on the wall for different loading ratios showed that they change approximately in proportion to this factor. The dependence of the same parameter on the particle diameter was studied for $\theta = 60^\circ$ and $\psi = 0.2$. Its values are almost coincident in the subsonic part of the nozzle, and there is a weak difference in the supersonic part: the maximum disagreement reaches 12%. Thus, we can conclude that the particle size has only a weak effect on the particle density on the wall.

Conclusions. Effective algorithms have been developed for computing the gas flow with solid particles in the inviscid flow core and in the boundary layer. The computed distributions of particle velocity at the centerline of a plane nozzle for different types of particles are in good agreement with experimental data. It is found that particles inserted in the subsonic part of the nozzle are accelerated by the gas and move away from the wall upstream of the nozzle throat. Then, they cross the centerline in the supersonic part of the nozzle and pass to the other half of the nozzle with respect to the centerline; particle focusing at the centerline is observed. An increase in particle concentration in the supersonic part of the nozzle leads to gas deceleration to a subsonic velocity. Later, the gas is again accelerated to a supersonic velocity. It is shown that different types of particle interaction with the wall lead to significant differences in distributions of particle parameters at the nozzle exit and have almost no effect on the axial distribution. It follows from the boundary-layer computations that the maximum of the particle density can be significantly higher than the density at the boundary-layer edge because of a significant decrease in cross-sectional area of the boundary layer in the subsonic part of the nozzle. During the motion in the supersonic part of the nozzle, this maximum approaches the wall, simultaneously decreasing in magnitude. It is found that the particle density on the wall depends weakly on the particle size and depends significantly on the half-angle of the subsonic part of the nozzle and on the loading ratio.

The authors are grateful to Prof. Krause and Prof. Olivier from the Technical University (Aachen, Germany) for their permanent attention to this work.

REFERENCES

1. B. Y. Wang and I. I. Glass, "Compressible laminar boundary layer flows of a dusty gas over a semi-infinite flat plate," *J. Fluid Mech.*, **186**, 223–441 (1988).
2. B. Y. Wang and I. I. Glass, "Boundary layer flows behind constant speed shock waves moving into a dusty gas," *Shock Waves*, **1**, No. 3, 135–144 (1991).
3. E. Outa, K. Tajima, M. Kobayashi, and S. Mimura, "Boundary layer of a non-equilibrium gas-particle mixture modified by particle lifting motion behind a shock front," in: *Proc. of the 17th Int. Symp. on Shock Waves and Shock Tubes* (Betlehem, PA, July 17–21, 1989), American Institute of Physics (1990), pp. 770–775.

4. R. Saurel, E. Daniel, and J. C. Loraud, "Two-phase flows: second-order schemes and boundary conditions," *AIAA J.*, **32**, No. 6, 1214–1221 (1994).
5. N. Thevand, E. Daniel, and J. C. Loraud, "On high-resolution schemes for solving unsteady compressible two-phase dilute viscous flows," *Int. J. Numer. Mech. Fluids*, **31**, 681–702 (1999).
6. N. Thevand and E. Daniel, "Numerical study of the lift force influence on two-phase shock tube boundary layer characteristics," *Shock Waves*, **12**, No. 4, 279–288 (2002).
7. S.-W. Kim and K.-S. Chang, "Reflection of shock wave from a compression corner in a particle-laden gas region," *Shock Waves*, **1**, No. 1, 65–73 (1991).
8. H. Sakakita, A. K. Hayashi, and A. I. Ivandaev, "Numerical simulation of shock wave interaction with powder layers," in: *Proc. of the 18th Int. Symp. on Shock Waves and Shock Tubes* (Sendai, Japan, July 21–26, 1991), Vol. 1, Springer-Verlag, Berlin–Heidelberg (1991), pp. 563–568.
9. B. Y. Wang, Q. S. Wu, C. Wang, et al., "Shock wave diffraction by a square cavity filled with dusty gas," *Shock Waves*, **11**, No. 1, 7–14 (2001).
10. T. R. Amanbaev, "Lifting of disperse particles from a cavity behind the front of an unsteady shock wave with a triangular velocity profile," *J. Appl. Mech. Tech. Phys.*, **44**, No. 5, 634–639 (2003).
11. I. M. Vasenin and A. D. Rychkov, "Numerical solution of the problem for a gas-particle flow in an axisymmetric Laval nozzle," *Izv. Akad. Nauk SSSR, Mekh. Zhidk. Gaza*, No. 5, 178–181 (1975).
12. A. A. Glazunov and A. D. Rychkov, "Nonequilibrium two-phase flows in axisymmetric Laval nozzles," *Izv. Akad. Nauk SSSR, Mekh. Zhidk. Gaza*, No. 6, 86–91 (1977).
13. L. E. Sternin, *Fundamentals of Gas Dynamics of Two-Phase Nozzle Flows* [in Russian], Mashinostroenie, Moscow (1974).
14. I. M. Vasenin, V. A. Arkhipov, V. G. Butov, et al., *Gas Dynamics of Two-Phase Nozzle Flows* [in Russian], Izd. Tomsk. Univ., Tomsk (1986).
15. A. D. Rychkov, *Mathematical Modeling of Gas-Dynamic Processes in Channels and Nozzles* [in Russian], Nauka, Novosibirsk (1988).
16. M. Sommerfeld, "Expansion of a gas/particle mixture in supersonic free jet flow," *Z. Flugwiss. Welraumforsch.*, **11**, No. 2, 87–96 (1987).
17. A. A. Mostafa, H. C. Mongia, V. G. McDonell, and G. S. Samuelsen, "Evolution of particle-laden jet flows: A theoretical and experimental study," *AIAA J.*, **27**, No. 2, 167–183 (1989).
18. N. N. Yanenko, R. I. Soloukhin, A. N. Papyrin, and V. M. Fomin, *Supersonic Two-Phase Flows under Conditions of Velocity Nonequilibrium of Particles* [in Russian], Nauka, Novosibirsk (1980).
19. H. C. Yee, R. F. Warming, and A. Harten, "Implicit total variation diminishing (TVD) schemes for steady-state calculations," *J. Comp. Phys.*, **57**, 327–360 (1985).
20. G. Seider, *Numerische Untersuchung Transsonischer Strömungen*, Aerodyn. Inst., RWTH, Aachen, Germany (1991).
21. A. N. Kraiko and S. M. Sulaimanova, "Two-fluid flows of a mixture of a gas and solid particles with "sheets" and "strings" arising in the flow around impermeable surfaces," *Prikl. Mat. Mekh.*, **47**, No. 4, 619–630 (1983).
22. R. F. Cuffel L. H. Back, and P. F. Massier, "Transonic flowfield in a supersonic nozzle with small throat radius of curvature," *AIAA J.*, **7**, 1364–1366 (1969).
23. V. N. Vetlutskii and V. L. Ganimedov, "Calculations of a compressible flow in a compression corner at high Reynolds numbers," *Aeromekh. Gaz. Dinam.*, No. 2, 10–20 (2003).
24. R. Courant, *Partial Differential Equations*, New York (1962).
25. V. M. Agranat and A. V. Milovanova, "Calculation of friction and heat transfer in a dusty boundary layer," in: *Mechanics of Reactive Media and Its Applications* [in Russian], Nauka, Novosibirsk (1989), pp. 164–170.
26. L. M. Vetlutskaya and V. N. Vetlutskii, "Calculation of a spatial compressible laminar boundary layer on a pointed body," in: *Numerical Methods of Mechanics of Continuous Media* (collected scientific papers) [in Russian], Vol. 17, No. 5, Inst. Theor. Appl. Mech., Sib. Div., Russian Acad. of Sci., Novosibirsk (1986), pp. 25–42.